Probing strong-field electron-nuclear dynamics of polyatomic molecules using proton motion

Alexei N. Markevitch,[1] Dmitri A. Romanov,[2] Stanley M. Smith,[1] and Robert J. Levis[1]
[1]*Department of Chemistry, Center for Advanced Photonics Research, Temple University, Philadelphia, Pennsylvania 19122, USA*
[2]*Department of Physics, Center for Advanced Photonics Research, Temple University, Philadelphia, Pennsylvania 19122, USA*
(Received 8 December 2006; published 3 May 2007)

Proton ejection during Coulomb explosion is studied for several structure-related organic molecules (anthracene, anthraquinone, and octahydroanthracene) subjected to 800 nm, 60 fs laser pulses at intensities from 0.50 to 4.0×10^{14} W cm^{-2}. The proton kinetic energy distributions are found to be markedly structure specific. The distributions are bimodal for anthracene and octahydroanthracene and trimodal for anthraquinone. Maximum (cutoff) energies of the distributions range from 50 eV for anthracene to 83 eV for anthraquinone. The low-energy mode ($\sim$10 eV) is most pronounced in octahydroanthracene. The dependence of the characteristic features of the distributions on the laser intensity provides insights into molecular specificity of such strong-field phenomena as (i) nonadiabatic charge localization and (ii) field-mediated restructuring of polyatomic molecules polarized by a strong laser field.

DOI: 10.1103/PhysRevA.75.053402 PACS number(s): 33.80.Rv, 31.50.Gh, 82.50.Pt

INTRODUCTION

The ongoing experiments on adaptive strong-field laser manipulation of chemical reactivity of polyatomic molecules make quantum control of matter a reality [1–8]. The strong-field experiments are performed in a laser intensity regime where dynamic Stark shift of molecular energy levels is on the order of level spacings. This strong-field interaction represents a new regime for control of molecular dynamics; its investigation is crucial for advances in manipulating matter with intense laser fields [9].

Ultrafast strong-field laser pulses cause multiple ionization and dissociation of polyatomic molecules through a process known as multielectron dissociative ionization [10]. In a common strong-field excitation scenario, a multiply ionized molecule "Coulomb explodes," and the fragments acquire large kinetic energies due to Coulomb repulsion. This process has been the subject of investigations covering a wide range of systems of various complexity from diatomic [10–12] to polyatomic [13,14] molecules, as well as atomic [15–17] and molecular [18,19] clusters.

The rational behind the Coulomb explosion mechanism is the effective separation of the ionization and dissociation stages: a molecule first rapidly loses several electrons and then the fragments are subsequently driven apart by Coulomb repulsion [10]. This simple model, however, becomes insufficient when nuclear motion is significant on the time scale of a laser pulse, i.e., when successive electronic excitations or ionizations occur as nuclei change positions. In this case, the electronic and nuclear degrees of freedom become strongly coupled during the laser-molecule interaction [14,20–24]. The coupled electronic nuclear motion regime poses significant challenges to theoretical modeling, numerical simulation, and interpretation of experimental results.

Previously, strong-field quantum-mechanical computations have been feasible only for systems of few electrons [25–28]. Recent advances in computational technology enable several groups to develop successful *ab initio* dynamical approaches to multielectron systems of polyatomic molecules in external fields [29–33]. However, because these approaches are computationally expensive, molecular dynamics investigations for pulse durations beyond a few fs have not been reported. Practically, for polyatomic molecules and atomic or molecular clusters of various degrees of complexity classical or semiclassical models still need to be developed to address laser intensities in the strong-field regime.

For reliable modeling and control of molecular dynamics, there are three generic regimes of laser-molecule coupling. They can be classified by relative magnitude of the ac Stark energy shifts and the characteristic energy level spacing of a molecule, Δ. The Stark shift can be quantified, for instance, by the free electron ponderomotive energy [34], $U_p = e^2E_0^2/(4m_e\omega^2)$ (here E_0 and ω are the laser field amplitude and frequency, respectively; m_e is electron mass, and e is the fundamental charge). The characteristic energy level spacing of the vast majority of polyatomic molecules falls into 5 ± 2 eV range; U_p is $\sim$6 eV at 10^{14} W cm^{-2} for the 800 nm field, and is linearly proportional to laser intensity.

In the $U_p/\Delta \ll 1$ regime (laser intensity $I < 10^{12}$ W cm^{-2}), the weak laser field causes resonant electronic transitions between well-defined field-free potential energy surfaces; the nuclear system evolves on these field-free surfaces. This regime has been extensively investigated, producing a number of important advances toward coherent control of electronic degrees of freedom and mode-selective chemistry [35–40]. However, resonant approaches are generally not well suited for control of nuclear motion in complex molecular systems [3,41]. This is because these approaches usually employ pulses whose duration is longer than intramolecular vibrational redistribution (IVR) times in polyatomics (the energy is redistributed over many vibrational modes at the same rate as it is deposited). To overcome this restriction, broadband mode-locked lasers have been used to attack a molecule with a sequence of short pulses [40] or to engage superposition of coherent pathways [38,39]. While restricted to the weak-field regime, these ingenious approaches are limited by inherent ineffectiveness of nonresonant laser-molecule coupling. To make a nonresonant interaction strong, one necessarily has to leave the realm of weak-field laser intensities.

 ©2007 The American Physical Society

In the case of ultrahigh laser intensities ($I \geq 10^{16}$ W cm^{-2}), where $U_p/\Delta \gg 1$, all polyatomic molecules are rapidly converted to miniplasma, in which the initial identity of a molecule is rapidly destroyed, and the electron-nuclear dynamics can be treated classically (Coulomb interaction among free electrons and ionic cores). In this $U_p/\Delta \gg 1$ regime the electron-nuclear dynamics is addressed by microplasma [42–44] or hydrodynamic [45] models. The control of nuclear dynamics in this regime is, however, hardly attainable, because the indiscriminate intensity of laser-molecule interaction completely overcomes individual details of the initial molecular Hamiltonian.

From the standpoint of control of nuclear motion, the most complex and interesting dynamics occurs at intermediate laser intensities ($I \sim 10^{13}$–10^{14} W cm^{-2}). In this $U_p/\Delta \sim 1$ regime, the strong laser field causes nonresonant, nonadiabatic electronic transitions between potential energy surfaces modified by the strong laser field to produce a quasicontinuum [23,46,47]. The initial stages of the electron-nuclear system's evolution occur on these field-dressed quasienergy surfaces [23]. The outcome of laser-molecule coupling is inherently sensitive not only to the details of molecular Hamiltonian but also to modification of the Hamiltonian by the strong-field laser pulse. Thus, we anticipate that this regime is most suitable for the manipulation of fragmentation dynamics.

Previously, we studied the electronic excitations of polyatomic molecules in the range of laser intensities that covers the transition from $U_p/\Delta \ll 1$ to $U_p/\Delta \sim 1$ regime. We reported that nonadiabatic electron dynamics in the latter regime is strongly molecule specific [46,47]. Here, we report the molecular specificity of nuclear motion during and after the interaction with the laser pulse. To this end we have measured the kinetic energies of protons ejected during photodissociation of a series of polyatomic molecules with particular focus on the kinetic energy release of H^+ formed in Coulomb explosion for three large polyatomic molecules–anthracene, ($C_{14}H_{10}$), 1,2,3,4,5,6,7,8-octahydroanthracene, ($C_{14}H_{18}$, OHA), and 9,10-anthraquinone, ($C_{14}O_2H_8$, anthraquinone). The structures of these molecules are shown in Fig. 1. The resulting molecule-specific proton kinetic energy distributions and corresponding insight into the dependence of the energy coupling process on the molecular structure is the subject of this paper.

EXPERIMENTAL

The experimental procedure has been briefly described previously [48]. Ion spectra were measured using a linear 1 m time-of-flight mass spectrometer in dual slope continuous extraction mode. A 1 mm aperture was placed between the ionization and detection regions of the spectrometer to restrict the signal collection to the near-focal cylindrical volume of the laser beam [49]. A regeneratively amplified Ti:sapphire laser [50] produced 10 Hz, 1.5 mJ, 60 fs pulses centered at 800 nm. The laser intensities were calibrated by comparison to the appearance thresholds for multiply charged argon.

Solid samples sublimed directly into vacuum to attain a pressure of $\sim 1 \times 10^{-6}$ Torr for anthracene and OHA, and

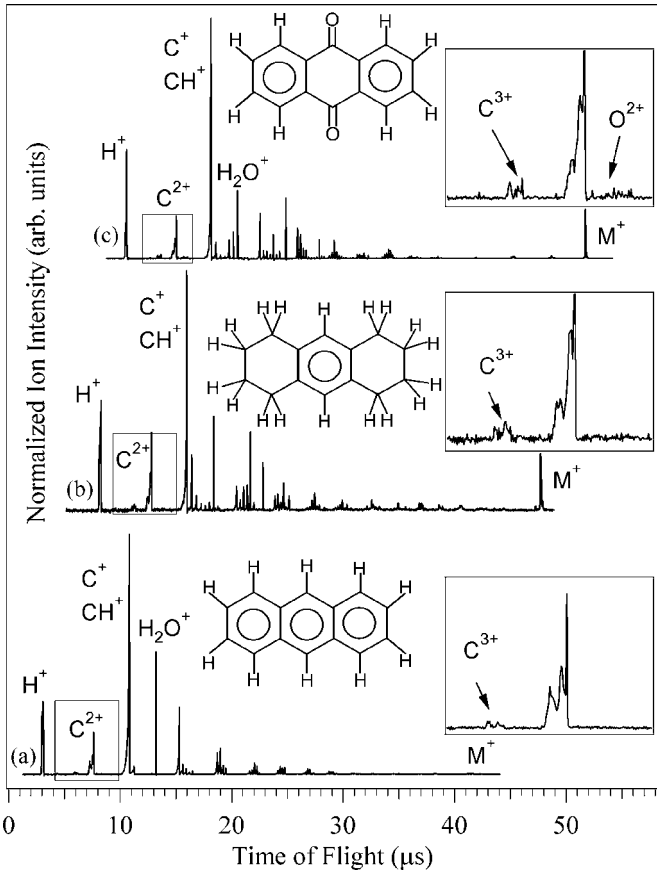

FIG. 1. Time-of-flight ion spectra of (a) anthracene, (b) 1,2,3,4,5,6,7,8-octahydroanthracene (OHA), and (c) 9,10-anthraquinone (anthraquinone) obtained using 800 nm, 60 fs laser pulses of laser intensity 3.5×10^{14} W cm^{-2}.

$\sim 10^{-7}$ Torr for anthraquinone; the background pressure for the spectrometer was $\sim 1 \times 10^{-8}$ Torr. These experiments were conducted at sufficiently low pressures to exclude possibility of space-charge interaction between individual molecules which affects the energy distributions of ion fragments formed in the process of Coulomb explosion. The H^+ signal from residual water molecules in the vacuum chamber constitutes only a very small fraction ($<1\%$) of the total proton signal observed. This was verified by collecting background spectra at $\sim 1 \times 10^{-8}$ Torr.

The kinetic energy distributions were measured in two complementary experiments. In the first, ions were allowed to drift ~ 5 mm in field-free conditions (prior to being extracted into the mass spectrometer by a +500 Volt potential), separating according to their initial velocities during the initial drift period. Thus, a smaller time of flight corresponds to a higher initial kinetic energy. In the second experiment, the kinetic energy distributions were exposed to a potential barrier before extraction into the time-of-flight system. This allows kinetic-energy calibration of the time-of-flight distributions because only those ions with sufficient energy to overcome the applied retarding potential are detected. Finally, the time-of-flight spectra H^+ obtained in the zero-field ion collection mode have been converted into kinetic energy distributions, using the calibrating retarding field measure-

ments and experimentally determined Jacobean intensity transformation from the time-of-flight to the kinetic energy scale. The intensity transformation accounted for the geometry of the spectrometer, the accelerating potentials and the delay between the ionization and the "time zero" of the time-of-flight spectra.

RESULTS

Figure 1 shows time-of-flight spectra of anthracene, OHA and anthraquinone obtained in the dual-slope extraction mode at the laser intensity $I=3.5\times10^{14}$ W cm^{-2}. The molecules are highly fragmented: the time-of-flight spectra contain H^+, C^{2+}, C^+, $^{13}C^+$, and/or CH^+, $C_2H_x^+$ peaks, followed by a manifold of heavier fragments $C_yH_x^+$, up to the corresponding parent ion, M^+. The spectra of OHA and anthraquinone show an appreciable amount of the parent ion signal. There are also minor peaks due to ionization of residual H_2O, N_2, and O_2 molecules. The insets to the spectra of anthracene and OHA show that the most highly charged fragment, C^{3+}, is just above the detection threshold at this laser intensity. The inset to the spectra of anthraquinone contains a peak corresponding to doubly charged oxygen, O^{2+}, the highest charge state of oxygen detected in this experiment. The O^{2+} signal is absent in spectra of anthracene and OHA, as shown in the corresponding inset to the spectrum of OHA. The relative amount of signal corresponding to $m/z=16u$ (O^+) is much higher in the spectrum of anthraquinone in comparison with that in the spectra of OHA and anthracene. This is expected since anthraquinone is the only molecule containing oxygen atoms. The spectrum of anthraquinone also contains a significant signal corresponding to $m/z=17u$, which we attribute to OH^+ formation from anthraquinone. (The small H_2O^+ and OH^+ signals in the spectra of anthracene and OHA are due to background water molecules in the time-of-flight chamber.)

All peaks at low m/z ratio are broadened due to kinetic energy acquired by the ions in the Coulomb explosion process. The peaks of the characteristic doublets correspond to the forward and backward components (relative to the direction of ion detection) of the ion velocity distributions. Although the most probable and cutoff kinetic energies of the ions can be estimated using the peak splitting of the time-of-flight spectra collected in the regular (dual slope extraction) mode, the combination of the field-free and retardation modes of ion detection described above provides much more detailed and precise information on the kinetic energy release.

Figures 2–4 show the forward component of the measured time-of-flight distributions of H^+ ejected from anthracene, OHA, and anthraquinone, respectively, as a function of laser intensity. The time-of-flight distributions exhibit nontrivial dependence on the laser intensity. For each molecule we observe two distinct regimes of H^+ expulsion dynamics. In the first regime, at lower laser intensities, the distributions are broad and featureless, and the total yield and the kinetic energy release of H^+ are strongly dependent on the intensity. In this regime, the total H^+ yield of these time-of-flight distributions increases rapidly, and the cutoff (minimum) and the

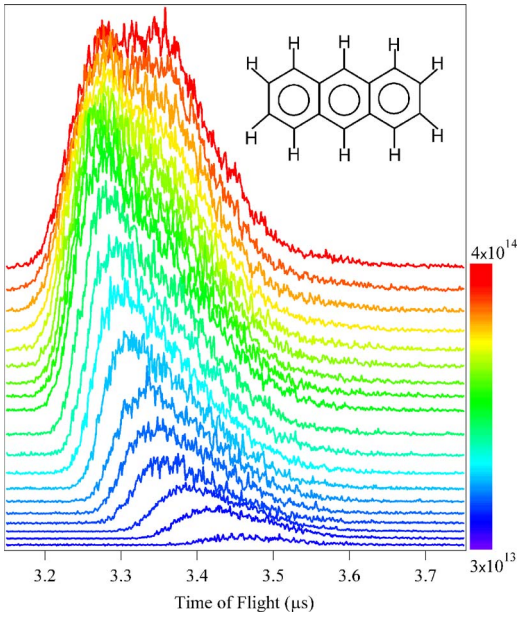

FIG. 2. (Color online) Time-of-flight distributions of H^+ ejected from anthracene at laser intensities from 0.50 to 4.0×10^{14} W cm^{-2}. The vertical offset is proportional to the increment in the laser intensity.

most probable values of these distributions decrease (indicating a higher kinetic energy release) with increasing laser intensity. Similar observations have been reported previously [48] for a series of four polycyclic aromatic hydrocarbons (benzene, naphthalene, anthracene, and tetracene) exposed to ~80 fs laser pulses of intensities up to 2×10^{14} W cm^{-2}. We observed [48] that at laser intensities above $\sim1.0\times10^{14}$ W cm^{-2} the energy coupling into the nuclear degrees of freedom begins to saturate. This saturation signifies

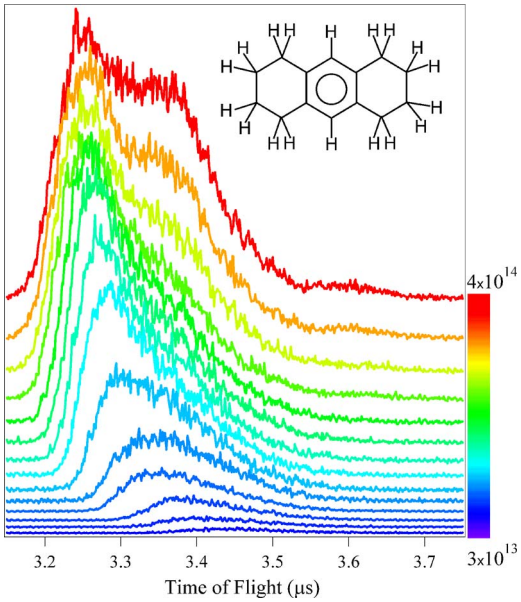

FIG. 3. (Color online) Time-of-flight distributions of H^+ ejected from OHA at laser intensities from 0.50 to 4.0×10^{14} W cm^{-2}. The vertical offset is proportional to the increment in the laser intensity.

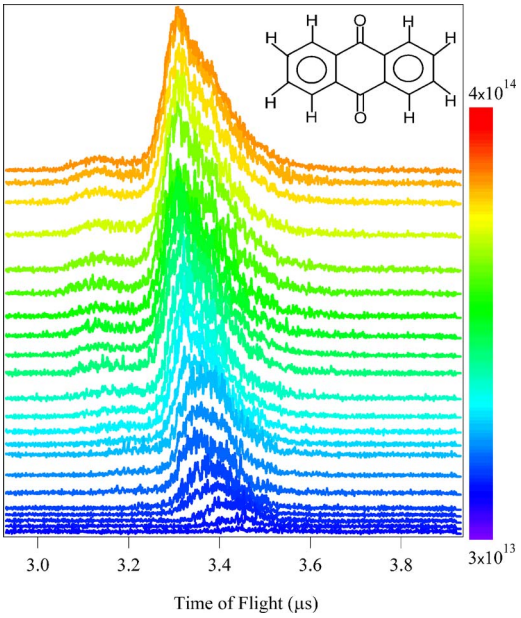

FIG. 4. (Color online) Time-of-flight distributions of H^+ ejected from anthraquinone at laser intensities from 0.20 to 2.50×10^{14} W cm^{-2}. The vertical offset is proportional to the increment in the laser intensity.

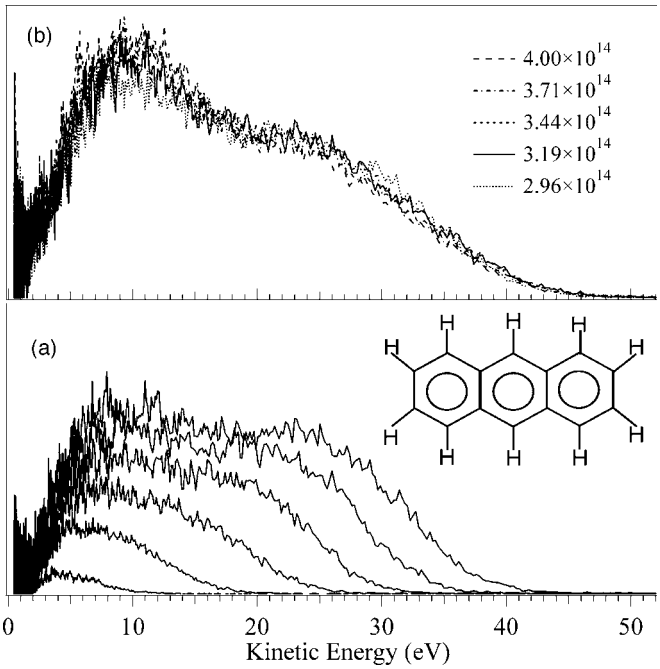

FIG. 5. (a) kinetic energy distributions of H^+ ejected from anthracene at laser intensities from 0.50 to 2.2×10^{14} W cm^{-2}. (b) H^+ energy distributions in the saturation regime.

the onset of the second regime of H^+ expulsion dynamics. To further explore the dynamics of polyatomic molecules in the saturation regime we increased the range of laser intensities up to 4.0×10^{14} W cm^{-2} in this experiment.

The time-of-flight distributions change remarkably with increasing laser intensity. The distributions are broad and featureless at lower laser intensities and split into several distinct modes with increasing intensity. Even cursory inspection reveals that the shapes of the distributions and the dependence on the laser intensity are clearly specific to the molecular structure; we will describe and quantify these differences later in terms of kinetic energy distributions derived from these data.

To convert the time-of-flight distributions shown in Figs. 2–4 to kinetic energy distributions of H^+ we calibrated the cutoff (minimum) values of the time-of-flight distributions using the retardation field measurements described above. We quantitatively assessed the kinetic energy corresponding to the shortest flight time of the expelled protons using the following procedure: (1) the time-of-flight spectra were converted to energy spectra using appropriate Jacobean transformation; (2) the standard deviation of the background noise of the energy spectra was calculated; (3) a boxcar average of 10 points was computed at the high-energy end of the spectrum to be used as the background average value for the signal; (4) the 10-point boxcar was moved one point toward lower energies, and the average value of the new position of the box was computed; (5) the new average value of the 10-point box was compared with the background average value. If the difference did not exceed two standard deviations of the background, step 4 was repeated. Otherwise, the middle point of the current box (the average energy of the box) was used as the cutoff energy, and the procedure was terminated.

The onset of the saturation regime is apparent in the dependence of the cutoff and most probable values of the time-of-flight distributions on the laser intensity: at higher laser intensities both the cutoff and the most probable values cease increasing and approach a limiting value. The retardation field measurements resulted in similar values of 50 ± 3 and $\sim52\pm3$ eV for the cutoff value of the kinetic energy releases for anthracene and OHA, respectively (at $I=4.0\times10^{14}$ W cm^{-2}). For anthraquinone, however, the retardation measurement resulted in the cutoff energy value of 83 ± 3 eV.

Figures 5–7 show kinetic energy distributions of H^+ ejected from anthracene, OHA, and anthraquinone, respectively for selected laser intensities. To aid the analysis we also plot maximum (cutoff) energy for these distributions vs laser intensity, Fig. 8. We observe large nonthermal kinetic energies of H^+ ions ejected from all three molecules. At lower intensities the energy distributions are broad and featureless. Both the most probable kinetic energy values and the cutoff energies increase rapidly (approximately linearly) with laser intensity. As the intensity exceeds $\sim1\times10^{14}$ W cm^{-2} this trend changes qualitatively. At $I\sim1.0\times10^{14}$ W cm^{-2} the distributions of anthracene and OHA become distinctly bimodal. For anthracene, the most probable values of the low-energy and the high-energy features increase with the laser intensity from 8 ± 1 eV and $\sim15\pm1$ eV at 1.1×10^{14} W cm^{-2} to 10 ± 1 eV and 25 ± 2 eV at 4.0×10^{14} W cm^{-2}, respectively. In the same laser intensity range the growth of the cutoff energy slows down and completely saturates reaching the value of 50 ± 2 eV at $I\sim3\times10^{14}$ W cm^{-2}. The laser intensity dependence of the H^+ kinetic energy distributions for OHA is similar to that of anthracene. At the maximum laser intensity of 4.0×10^{14} W cm^{-2} the most probable values of the low and high-energy features are 10.0 ± 1.0 eV and 26 ± 1.0 eV, re-

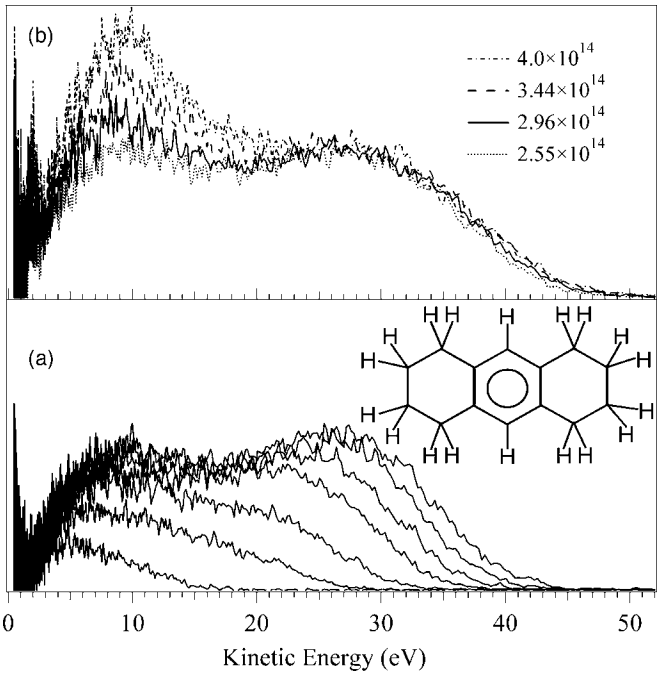

FIG. 6. (a) kinetic energy distributions of H^+ ejected from OHA at laser intensities from 0.50 to 2.2×10^{14} W cm^{-2}. (b) H^+ energy distributions in the saturation regime.

spectively. The kinetic energy distribution of OHA possesses a small low-energy feature centered at 2.0 ± 0.25 eV (not present in anthracene). This feature, absent at lower laser intensities, becomes more prominent as the intensity exceeds $\sim2.5\times10^{14}$ W cm^{-2}.

The laser intensity dependence of the H^+ kinetic energy distribution for anthraquinone is significantly different from

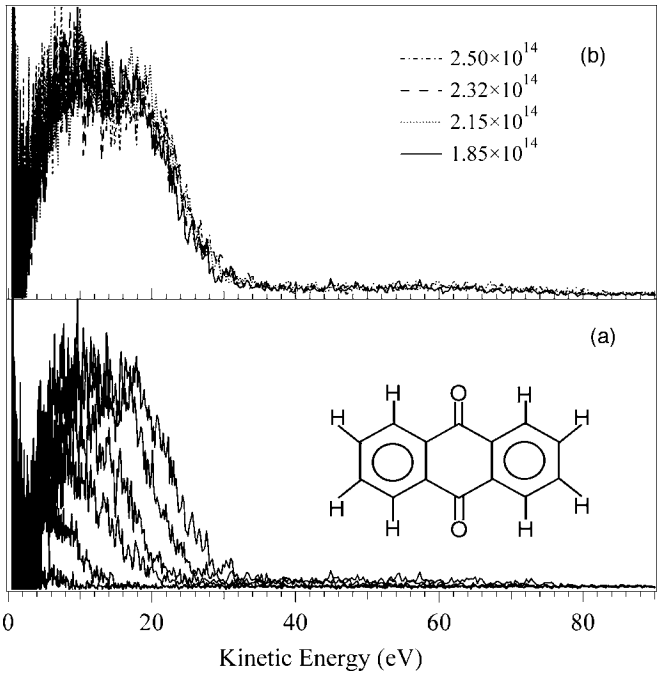

FIG. 7. (a) kinetic energy distributions of H^+ ejected from anthraquinone at laser intensities from 0.20 to 1.85×10^{14} W cm^{-2}. (b) H^+ energy distributions in the saturation regime.

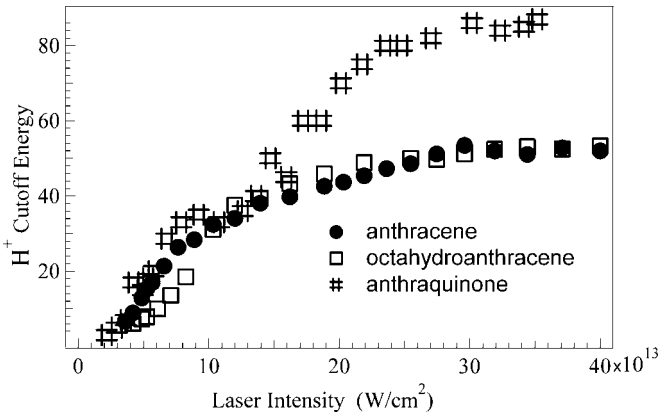

FIG. 8. The cutoff kinetic energies (eV) of the H^+ kinetic energy distributions for (a) anthracene, (b) OHA, and (c) anthraquinone as a function of laser intensity, W cm^{-2}.

that of anthracene and OHA. From $I=2.0\times10^{13}$ up to $\sim8.0\times10^{13}$ W cm^{-2} the distributions are characterized by a single mode with both the cutoff and most probable values increasing rapidly with the laser intensity. As the intensity increases, three distinct features emerge in the kinetic energy distributions of anthraquinone. At $I\sim9.0\times10^{13}$ W cm^{-2} a high-energy feature with a cutoff value extending to approximately 83 ± 3 eV (at the highest laser intensities) begins to form. The rest of the distribution, containing most of the H^+ signal, splits into two features, with most probable values of ~10 and ~18 eV at $I\leq2.5\times10^{14}$ W cm^{-2}.

DISCUSSION

When hydrocarbon molecules are subjected to short intense laser pulses, the expulsion of H^+ is expected to occur much faster than disintegration of the carbon skeleton. This is because (i) heavier C atoms take longer time than protons to accelerate in the Coulomb field, (ii) C atoms form four bonds while an H atom forms only one bond, and (iii) protons occupy peripheral positions in a molecule. The protons, ejected from much heavier counter ions, carry most of the kinetic energy of the Coulomb explosion, which is partitioned between the ejected H^+ and the counter ion. If, under these conditions, the light H^+ ions pick up the majority of the kinetic energy release on the time scale of the laser pulse, the H^+ kinetic energy distribution becomes a signature of the dynamics of energy deposition and fragmentation, reflecting the details of both the molecular structure and the laser pulse properties. The data presented here suggest that measurements of the energy distributions of the H^+ formed in the process of the Coulomb explosion of large organic molecules should become an important tool for studying the strong-field electron-nuclear dynamics of energy deposition and molecular fragmentation.

The origin of the features of the proton energy distributions and the dependence of the distributions on the laser intensity should be attributable to the nuclear structure of the molecule. The framework of these three molecules is similar and is formed by three fused polycyclic six-carbon rings. These molecules have the same number of carbon atoms and

have similar spatial dimensions. Anthracene and anthraquinone are rigorously planar (and have the same D_{2h} symmetry). Geometry optimization of OHA [using GAUSSIAN03 (Ref. [51]] reveals that the molecule is slightly twisted due to the sp^3 type bonding of the outer carbon rings; this molecule is of a lower C_2 symmetry. The three molecules differ substantially in the extent of their conjugated π-electron systems. In the case of anthracene the 14 π electrons are delocalized over the entire polycyclic structure. In the case of anthraquinone, the conjugation extends only over the two terminal rings with 6 π electrons each. The central ring in anthraquinone forms a substantial barrier for the π-electron motion. In the case of OHA, the 6π-electron system resides on the central ring, while the terminal rings are fully saturated with H atoms. One major difference between anthraquinone and the other two molecules is the presence of the carbonyl groups at the 9 and 10 positions of the carbon skeleton. These highly electronegative oxygen atoms create the barrier for the π electrons and will play a pivotal role in strong-field electron dynamics. Overall, although the carbon backbones are similar in all three molecules, the H atoms find themselves in different chemical environments, as is clearly revealed by NMR spectra of these molecules [52,53].

The kinetic energy distributions of protons released from these three polyatomic molecules reveal an initial rapid growth with increasing laser intensity followed by the eventual onset of the saturation of the kinetic energy release. We also observe that these distributions possess distinct molecule-specific features. Thus, two main areas of inquiry arise regarding the dynamics of H^+ expulsion during fragmentation of these molecules. First, we need to understand the origin of the rapid growth of the H^+ kinetic energy with increasing laser intensity and the eventual onset of the saturation of the kinetic energy release. Second, the dependence of features in the kinetic energy distributions on molecular structure should be addressed.

One of the important observations in this experiment is the rapid growth of the measured H^+ maximum kinetic energy at $I < \sim 10^{14}$ W cm^{-2} for all three molecules. For example, in the case of anthracene, the H^+ cutoff energy grows from 8 to 30 eV as the laser intensity increases from 0.4 to 1.0×10^{14} W cm^{-2}. In a recent publication [23] we have analyzed the mechanism of formation of the highly energetic protons during ionization and dissociation of anthracene and concluded that Coulomb explosion of anthracene is accompanied by nonadiabatic charge localization. In the experiments presented here, each of the three molecules produces highly energetic protons in the laser intensity regime $U_p \sim \Delta$. The evolution of the high-energy features in the distributions as a function of increasing laser intensity is explained by a Coulomb explosion mechanism that involves nonadiabatic charge localization. This phenomenon emerges as generic in coupling of large organic molecules with strong laser fields.

In the nonadiabatic charge localization model, a series of nonadiabatic electronic Landau-Dykhne type transitions [54] occur during successive multiple ionization and dissociation events in a polyatomic molecule. Although anthracene has D_{2h} symmetry (the charge transfer states are initially nearly degenerate), in the early stages of the excitation this degeneracy can be broken due to accompanying asymmetric nuclear motion. As a result, the positive charge is localized at one of the ends of the molecule for a significant portion of the laser pulse. The protons ejected from the more positive end of the molecule acquire kinetic energy that exceeds that anticipated from the simple Coulomb explosion picture. The model of dissociative ionization, assisted by prolonged nonadiabatic charge localization successfully explained the measured anthracene H^+ kinetic energy dependence on the laser intensity.

The proton energy distributions for OHA are similar to that for anthracene. The main difference is the more pronounced growth of the low-energy part of the distribution for OHA in comparison with anthracene as the laser intensity approaches the saturation regime. As discussed previously, [23,24] the low-energy ($\sim$10 eV) feature in anthracene and anthraquinone can be explained by simple Coulomb explosion considerations without invoking charge localization arguments. Similarly, in the case of OHA, the charge localization is expected to be most effective for molecules whose longest (active) axis is parallel to the direction of polarization of the laser field. These heavy molecules are not appreciably aligned by the laser field, and therefore essentially retain the original random distribution relative to the field during the laser pulse. As was the case with anthracene, the low-energy feature in OHA can be attributed to H^+ expulsion from molecules whose short in-plane axis is oriented along the laser electric field vector. Because the low-energy protons are due to average ionic charge and have no relation to the localization phenomenon, their formation continues even when the localization (responsible for the high-energy features) saturates. The growth of the lower ($\sim$10 eV) energy feature with increasing laser intensity for OHA is much more prominent in comparison with the corresponding feature for anthracene and anthraquinone. This may indicate that the fraction of molecules not affected by charge localization is greater for OHA in comparison with that of anthracene or anthraquinone. Thus, there are more hydrogen atoms in OHA that are not affected by the charge localization. This is consistent with the reduced symmetry and electron delocalization of OHA.

A proton experiences the Coulomb forces from positive charges distributed over the multiply charged molecular ion during ejection. Accordingly, the proton kinetic energy distribution is determined by the total charge on the molecule, the size of the molecule (i.e., the average distance between the proton in question and the distributed positive charge), and the molecular symmetry (possible directions of the proton expulsion). Since all the three molecules are of approximately same size, their size is not a factor of considerable distinction. The relative degree of ionization of the three molecules as a function of laser intensity can be extrapolated from nonadiabatic multielectron dynamics calculations [46,47] (see Table I). These calculations predict the following order of the relative degree of ionization of molecules aligned with the laser electric field: anthracene $>$ anthraquinone $>$ OHA. Note, however, that the ionization yield for anthracene is much more anisotropic than for the other two molecules. The order of ionization yield curves is corroborated by our previous experiments at lower laser intensities [46,47].

TABLE I. Electronic properties of neutral molecules and +1 molecular ions calculated using GAUSSIAN03. The transition dipole moments, characteristic transition energies, and dynamic polarizabilities of the ground states of neutral molecules and the molecular ions of anthraquinone and anthracene.

Molecular formula/ laser field orientation	μ, e Å, neutral (ion)	Δ, eV, neutral (ion)	α (800 nm), e Å^2 V^{-1}, neutral (ion)	Double ionization rate at 2×10^{14} W cm^{-2} peak laser intensity
$C_{14}H_8O_2$, long axis	0.62 (0.77)	5.11 (3.54)	2.53 (2.80)	0.393
$C_{14}H_8O_2$, O-O axis	1.00 (0.60)	4.57 (4.27)	1.80 (1.62)	0.253
$C_{14}H_{10}$, long axis	2.10 (1.91)	5.17 (5.13)	3.02 (5.13)	0.535
$C_{14}H_{10}$, short axis	1.09 (1.10)	6.87 (6.90)	1.65 (1.71)	0.0104
$C_{14}H_{18}$, long axis	0.711 (1.04)	6.14 (6.37)	2.11 (2.72)	0.0477
$C_{14}H_{18}$, short axis	0.471 (0.516)	6.21 (5.95)	1.59 (1.61)	0.0164

Analysis of the proton detection probability in the given mass-spectrometer geometry suggests that for randomly oriented molecules comparatively more low-energy protons should be detected in the case of OHA. The molecular symmetry of OHA (C_2) is reduced in comparison with that of anthracene and anthraquinone (D_{2h}). For anthracene and anthraquinone, all of the atoms are in the molecular plane. The outgoing motion of the ejected protons does not deviate much from this plane, so if the plane is oriented at appreciable angle with respect to the electric field/detector tube, virtually no protons will be registered. OHA is more complicated because this molecule is not strictly planar (having only C_2 symmetry). The carbons of the terminal rings have sp^3 hybridization and thus form slightly twisted rings. The protons attached to these sp^3 carbons are completely out of plane, their bonds pointing out at tetrahedral angle, see Fig. 9. This structure makes for much wider spatial angle of possible proton detection.

The probability of detection of an outgoing proton depends on the orientation of the molecule with respect to the time-of-flight tube. In the reported experiment the laser field is horizontally polarized, and the detector is in the plane of polarization. The molecules are randomly oriented and are not appreciably aligned during the pulse. Thus, when the electric field is normal to the molecular plane of anthracene and anthraquinone, virtually no protons should be detected, while OHA has more orientations with respect to time-of-flight axis resulting in proton detection. Anthracene and OHA should have similar high-energy proton expulsion features. We expect the high-energy protons to result from molecules in which effective charge localization occurs, i.e., from those molecules whose long axis is aligned with the electric field of the laser. There should be the same number of such molecules in randomly oriented sets of anthracene and OHA. Similarly, the lower-energy proton expulsion features are expected to result from those molecules whose long axis is not aligned with the electric field of the laser. As OHA more effectively couples with the field in such orientations due to its reduced symmetry, the lower-energy feature of OHA shows more pronounced growth at higher laser intensities in comparison with that of anthracene.

A small feature at ~2 eV is observed in OHA but is absent in anthracene and anthraquinone (Figs. 5–7, panel B). Although this feature appears in OHA only at higher laser intensities, the formation of 2 eV protons does not require significant Coulomb repulsion. Such protons may result from post pulse dissociation of electronically excited fragments containing unbroken C-H bonds. Because there are more C-H bonds in the OHA in comparison with anthracene or anthraquinone, these fragments are expected to be more abundant in OHA in comparison with the other two molecules, as observed.

The high-energy features (peaking at ~25 eV) appear to be very similar in OHA and anthracene (the cutoff energy of OHA seem to be slightly larger than for anthracene: ~52 eV vs ~50 eV). Some difference can be seen in more gradual

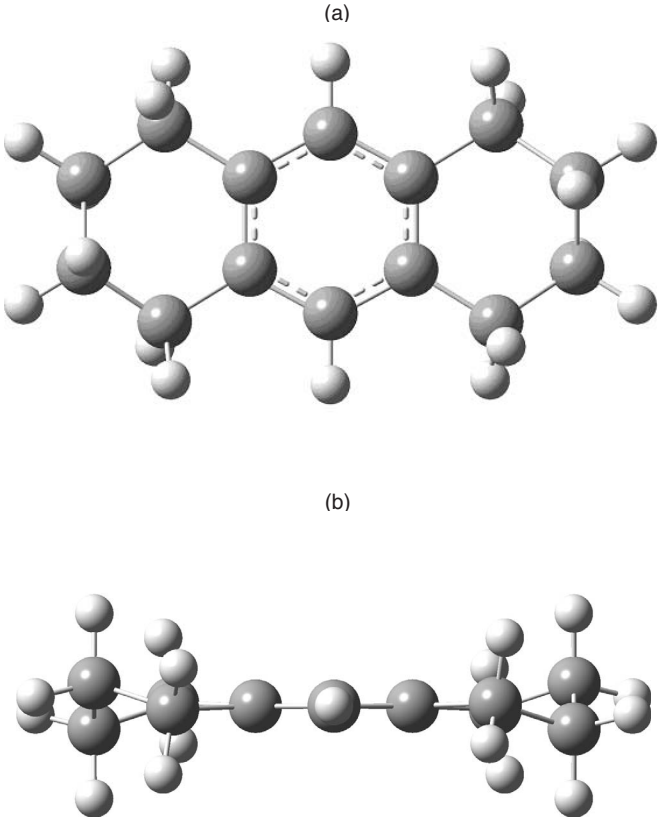

FIG. 9. Molecular structure of 1,2,3,4,5,6,7,8-octahydroanthracene. (a) view in the direction normal to the central-ring plane; (b) view along the short in-plane axis. Note the out-of-plane hydrogen atoms on the terminal rings.

approach of anthracene to the saturation regime (see Fig. 8). The difference can be possibly attributed to a larger amount of charge screening in OHA in comparison with anthracene at lower laser intensities.

The proton energy distributions for anthraquinone are significantly different from that of anthracene and OHA. In the trimodal distribution of anthraquinone, the second feature (centered at 18 eV, cutoff at ~40 eV) originates, as previously discussed, in laser coupling along the long axis. It is comparable to the high-energy features of anthracene and OHA (both centered at 25 eV, cutoff at 50–52 eV). Since these modes of the distributions are expected to result from laser coupling along the long axis of all three molecules, it is instructive to understand how these molecular structures provide similar proton energies for anthracene and OHA and why the proton energies for anthraquinone are lower.

In Fig. 8 the proton cutoff energies for anthracene and OHA differ at lower laser intensities (the cutoff energy for anthracene initially increases faster than for OHA) but practically merge at the higher laser intensities. This convergence of the maximum proton expulsion energies for structurally different molecules may be viewed as surprising. However, as the degree of ionization increases, the structural differences between the two molecules have progressively smaller impact on the charge localization process.

The resulting energies of the protons ejected from these two molecules are ultimately determined by the nonadiabatic charge localization along the long molecular axis. This localization is conditioned by the ability of electric charge to move from one end of the molecule to the other. Polarizability of a molecule is a natural measure of this ability; from this standpoint, anthracene and OHA differ by their degree of π-electron conjugation. The polarizability of anthracene (neutral and +1 molecular ion) is measurably larger than that of OHA (see Table I). Therefore one expects more pronounced localization of charge in anthracene, and consequently ejection of more energetic protons from this molecule. Structural/electronic properties of these two molecules also suggest that anthracene will be more readily ionized at the lower laser intensities producing +1(+2) ions (this is corroborated by our multielectron dynamics calculations for these two molecules). In accord with these expectations, anthracene shows faster growth of the proton cutoff values when compared to those for OHA at the lower laser intensities that correspond to the initial stages of electronic excitation and ionization (see Fig. 8).

With increasing laser intensity, the anthracene and OHA curves in Fig. 8 practically merge, as the degree of ionization increases from +1(+2) to +3(+4). This suggests that as the laser intensity increases, the degree of ionization and the charge distribution become more similar for these two molecules. Using GAUSSIAN03, we calculated charge distributions over constituent atoms in neutral molecules and their ions of increasing degree of ionization. These distributions show that in +1 molecular ion of anthracene the positive charge is delocalized more evenly over the whole molecule, while in OHA the positive charge is delocalized mostly over the central aromatic ring. With an increasing degree of ionization, the additional positive charge in both anthracene and OHA concentrates predominantly on the terminal rings, producing charge distribution picture essentially similar in both molecules. Thus, at higher degree of ionization, the two molecules manifest progressively similar charge-distribution response to strong laser field, despite considerable differences in electronic properties of neutral molecules.

Unlike anthracene and OHA, anthraquinone has an effective barrier preventing electron motion from one side of the molecule to the other side through the central ring. This barrier impedes the charge oscillations in the anthraquinone ion in a strong field making for lower charge available for localization. This weakened localization results in the observed ~20% shift of the second mode of the proton kinetic energy distribution to lower energies. Note the characteristic difference in the roles that the central ring plays in anthraquinone and OHA. In OHA, the central aromatic ring does not disrupt but rather improves the communication between the terminal rings. This mediates charge delocalization in the ion and makes for more effective charge localization on one of the terminal rings.

The foregoing discussion emphasized the important fact that the proton kinetic energy distributions of these molecules are signatures of field-dressed molecules that only reveal themselves in the strong-field regime. As such, the observed differences in the distributions cannot be predicted based exclusively on weak-field molecular electronic parameters (such as polarizability, ionization potential, magnitude of energy gaps between various electronic states, and corresponding transition dipole moments). This shows once more that strong-field properties of a molecule are complementary to its weak-field properties and cannot be reduced to them.

Finally, we address the most interesting structure-specific high-energy feature of anthraquinone proton kinetic energy distributions (up to 83 eV, see Figs. 4 and 7); this feature is absent in either anthracene or OHA. Since anthraquinone is the only molecule in this series containing oxygen, and the high-energy feature is specific to anthraquinone, we attribute the formation of this feature to intramolecular interaction of anthraquinone protons with oxygen. We propose that the oxygen atoms are highly polarized by the charge localization during the laser pulse and contribute to the formation of these high-energy protons.

Although oxygen atoms in anthraquinone can be polarized to harbor a significant transient positive charge, in the ground-state geometry they are still separated from the closest protons by ~1.5 Å, which seems to be too great a distance to explain the formation of the most energetic protons. It is known, however, that structures similar to anthraquinone may exist in an isomeric zwitterionic form. The formation of the isomer would happen if an H atom adjacent to oxygen migrated from the carbon of the aromatic ring to form a bond with the oxygen. In the zwitterion a partial negative charge would be delocalized over the aromatic ring (from which the proton had migrated) and a counter positive charge would reside on the oxygen atom accepting the proton.

In our previous paper [24] we modeled possible formation of anthraquinone zwitterion by optimizing its structure using GAUSSIAN03 [B3LYP density-functional method with a 6-311G(d) basis set]. Although computations reveal a shallow (less than 0.1 eV deep) high-lying (~6.8 eV) local potential energy minimum for a proton near oxygen, our analy-

sis has also shown that such an isomer of anthraquinone cannot be formed under normal gas phase conditions on either the ground or electronically excited potential energy surfaces.

However, the electric field of the laser causes redistribution of the electron density within the molecule and the molecular ion of anthraquinone, substantially changing the nuclear potential energy surfaces during the laser pulse, which in turn can cause restructuring of the molecule prior to Coulomb explosion. The restructuring is predicted by a numeric model [24] in which charge redistribution in the molecule under the influence of a strong field results in transient forces on the nuclei, inducing fast proton migration toward a field-dressed potential energy minimum near an oxygen atom.

To model the intramolecular proton motion under the action of strong oscillating forces of the polarized charge, we reduced the H^+ potential surface to one dimension. The model potential curve reproduces the two main features of the H^+ potential energy surface, i.e., the deep minimum of the equilibrium position and a weak isomeric minimum,

$$V(z) = V_0\left(\frac{1}{4}z^4 - \frac{3}{2}z^2 + 2(1-\gamma)z\right). \tag{1}$$

Here, $z=x/x_0$ is the dimensionless variable, V_0, x_0, and γ are fitting parameters to model energy splitting between the ground-state and the isomer structure ($\Delta E=6.8$ eV), the interminimum spatial distance ($\Delta x \approx 2.5$ Å), and the frequency of the proton oscillations near the equilibrium minimum ($\omega_0=0.63$ fs^{-1}) [55]. The parameter γ is small to ensure that the isomeric minimum is shallow.

Within this model, the dimensionless equation of motion of the proton driven by the oscillating force with frequency ω is given by

$$(9-8\gamma)\frac{d^2z}{d\tau^2} = -z^3 + 3z + 2(1-\gamma) + 2\frac{\Delta x}{\Delta E} \times\left(\frac{9}{8} - \frac{8}{9}\gamma - \sqrt{\frac{3}{2}\gamma}\right) f(z,\beta\tau), \tag{2}$$

where $\tau=\omega_0 t$, $\beta=\omega/\omega_0$. The effective oscillating force $f(z,\beta\tau)$ acting along the reaction coordinate z consists of two terms that represent the alternating H-O Coulomb drag and H-C bond softening induced by the polarization in the laser field applied in the direction parallel to the line connecting the oxygen atoms. For one half-cycle of the laser field oscillations, when the H^+ under consideration is on the positive side of the molecule, the C-H bond is softened. During the next half-cycle, the negative charge on oxygen atom attracts H^+. The alternating actions of the bond softening and the strong attraction extract the H^+ out of its equilibrium position and propel it to the isomeric minimum.

We numerically solved Eq. (2) using structural and electronic parameters of anthraquinone [51]. The behavior of H^+ depends qualitatively on the strength of the oscillating electric field. In a relatively small field, the proton oscillates near the equilibrium position with a period characteristic of C-H bond vibration (~10 fs). As the field strength grows, these oscillations become more complex, but H^+ is still confined near the equilibrium minimum. However, when the field exceeds a threshold of about 2.5 V/Å, the trajectory undergoes a transition to large-amplitude oscillations centered at the higher isomeric minimum. Depending on the field strength, the H^+ transfer to the field-dressed minimum takes 25 fs or less. Thus, the restructuring of the molecule can occur before the Coulomb explosion expels the H^+ with high kinetic energy.

Another corroborating piece of evidence for the intramolecular proton transfer is the observation of OH^+ ion in the spectra of anthraquinone, see Fig. 1(c). We have conducted an additional experiment to verify that the observed OH^+ signal results from anthraquinone molecule and not from any water molecules that might accompany the solid anthraquinone sample or occur in the chamber background. Specifically, we have heated the chamber containing the sample of anthraquinone (up to 100 °C) and monitored the amount of water signal in the anthraquinone spectra, as well as the shape of the H^+ distribution. As the chamber is heated, initially the amount of detected water and OH^+ signal increases significantly, indicating drying of the hygroscopic solid anthraquinone sample and desorption of water molecules from the walls of the chamber. The H_2O^+ signal remains high for about 30 min, and then decreases to much lower levels comparable to those of background water without anthraquinone sample in the chamber (at the relevant temperature). However, the shape of the H^+ distribution is not affected by the heating of the chamber, and the amount of OH^+ remains relatively higher than could be expected from dissociation of background H_2O and comparable to that observed before heating.

Field-driven restructuring of anthraquinone structure occurring prior to the Coulomb explosion explains how protons come into a close proximity to oxygen before being subsequently ejected with high kinetic energy. Thus, the H^+ kinetic energy distributions of anthraquinone can be understood as follows. The lower energy modes of the distributions (<50 eV) result from processes analogous to that discussed previously for anthracene [23]. The high-energy mode specific for anthraquinone (extending up to ~83 eV at the highest laser intensity) is the result of H^+ expulsion following the intramolecular transfer into the field-dressed metastable minimum.

CONCLUSIONS

The energy distributions of the protons resulting from the dissociative ionization of three polyatomic molecules subjected to strong near IR laser pulses reveal system-specific characteristics of the pulse-driven fragmentation process. The laser intensity regime $U_p \sim \Delta$ proves to be favorable for uncovering the molecular structure effects on the strong-field electron-nuclear dynamics. The measured proton kinetic energy distributions depend sensitively on the molecular structure, although the observed differences in the distributions cannot be predicted based exclusively on the weak-field mo-

lecular electronic parameters (such as polarizability, Δ, ionization potential). It is shown that the proton kinetic energy distributions are signatures of field-dressed molecules that only reveal themselves in the strong-field regime. The characteristic features of the proton energy distributions are explained in terms of nonadiabatic charge localization and field-mediated restructuring. Measurements of the energy distributions of the protons released in the process of Coulomb explosion of large organic molecules should become important tool for studying the strong-field electron-nuclear dynamics of energy deposition and molecular fragmentation. Utilization of these processes can open new prospects for effective quantum control of strong-field molecular fragmentation and reactivity.

ACKNOWLEDGMENTS

The authors would like to gratefully acknowledge financial support of the NSF, ONR, and the DOD MURI program as administered by the U. S. Army Research Office.

[1] R. S. Judson and H. Rabitz, Phys. Rev. Lett. **68**, 1500 (1992).
[2] M. M. Wefers and K. A. Nelson, Science **262**, 1381 (1993).
[3] R. J. Levis, G. M. Menkir, and H. Rabitz, Science **292**, 709 (2001).
[4] B. J. Pearson, J. L. White, T. C. Weinacht, and P. H. Bucksbaum, Phys. Rev. A **63**, art. no. 063412 (2001).
[5] S. M. Hurley and A. W. Castleman, Science **292**, 648 (2001).
[6] E. Wells, K. J. Betsch, C. W. S. Conover, M. J. DeWitt, D. Pinkham, and R. R. Jones, Phys. Rev. A **72**, 063406 (2005).
[7] C. Trallero-Herrero, D. Cardoza, T. C. Weinacht, and J. L. Cohen, Phys. Rev. A **71**, 013423 (2005).
[8] I. V. Hertel and W. Radloff, Rep. Prog. Phys. **69**, 1897 (2006).
[9] R. J. Levis and H. A. Rabitz, J. Phys. Chem. **106**, 6427 (2002).
[10] L. J. Frasinski, K. Codling, P. Hatherly, J. Barr, I. N. Ross, and W. T. Toner, Phys. Rev. Lett. **58**, 2424 (1987).
[11] S. Chelkowski and A. D. Bandrauk, J. Phys. B **28**, L723 (1995).
[12] C. Cornaggia, J. Lavancier, D. Normand, J. Morellec, P. Agostini, J. P. Chambaret, and A. Antonetti, Phys. Rev. A **44**, 4499 (1991).
[13] S. Shimizu, J. Kou, S. Kawato *et al.*, Chem. Phys. Lett. **317**, 609 (2000).
[14] M. Tchaplyguine, K. Hoffmann, O. Duhr *et al.*, J. Chem. Phys. **112**, 2781 (2000).
[15] T. Ditmire, J. W. G. Tisch, E. Springate, M. B. Mason, N. Hay, J. P. Marangos, and M. H. R. Hutchinson, Phys. Rev. Lett. **78**, 2732 (1997).
[16] T. Ditmire, R. A. Smith, J. W. G. Tisch, and M. H. R. Hutchinson, Phys. Rev. Lett. **78**, 3121 (1997).
[17] V. P. Krainov and S. P. Roshchupkin, Laser Phys. **12**, 375 (2002).
[18] J. V. Ford, Q. Zhong, L. Poth *et al.*, J. Chem. Phys. **110**, 6257 (1999).
[19] V. P. Krainov and A. S. Roshchupkin, Phys. Rev. A **64**, 063204 (2001).
[20] T. Seideman, M. Y. Ivanov, and P. B. Corkum, Phys. Rev. Lett. **75**, 2819 (1995).
[21] T. Zuo and A. D. Bandrauk, Phys. Rev. A **52**, R2511 (1995).
[22] V. R. Bhardwaj, P. B. Corkum, and D. M. Rayner, Phys. Rev. Lett. **91**, 203004 (2003).
[23] A. N. Markevitch, D. A. Romanov, S. M. Smith, and R. J. Levis, Phys. Rev. Lett. **92**, 063001 (2004).
[24] A. N. Markevitch, D. A. Romanov, S. M. Smith, and R. J. Levis, Phys. Rev. Lett. **96**, 163002 (2006).
[25] S. Chelkowski, T. Zuo, O. Atabek, and A. D. Bandrauk, Phys. Rev. A **52**, 2977 (1995).
[26] S. Chelkowski, C. Foisy, and A. D. Bandrauk, Phys. Rev. A **57**, 1176 (1998).
[27] H. T. Yu, T. Zuo, and A. D. Bandrauk, J. Phys. B **31**, 1533 (1998).
[28] A. D. Bandrauk, S. Chelkowski, and I. Kawata, Phys. Rev. A **67**, 013407 (2003).
[29] E. Deumens and Y. Ohrn, J. Phys. Chem. A **105**, 2660 (2001).
[30] P. Krause, T. Klamroth, and P. Saalfrank, J. Chem. Phys. **123**, 074105 (2005).
[31] X. S. Li, S. M. Smith, A. N. Markevitch *et al.*, Phys. Chem. Chem. Phys. **7**, 233 (2005).
[32] E. Gindensperger, I. Burghardt, and L. S. Cederbaum, J. Chem. Phys. **124**, 144103 (2006).
[33] X. S. Li, J. C. Tully, H. B. Schlegel *et al.*, J. Chem. Phys. **123**, 084106 (2005).
[34] T. W. B. Kibble, Phys. Rev. Lett. **16**, 1054 (1966).
[35] K. Bergmann, H. Theuer, and B. W. Shore, Rev. Mod. Phys. **70**, 1003 (1998).
[36] A. H. Zewail, J. Phys. Chem. A **104**, 5660 (2000).
[37] A. H. Zewail, J. Phys. Chem. **100**, 12701 (1996).
[38] P. Brumer and M. Shapiro, Laser Part. Beams **16**, 599 (1998).
[39] M. Shapiro and P. Brumer, in *Advances in Atomic Molecular, and Optical Physics*, edited by B. Bederson and H. Walther(Academic Press, San Diego, 2000), Vol. 42, p. 287.
[40] D. J. Tannor and S. A. Rice, Adv. Chem. Phys. **70**, 441 (1988).
[41] H. Rabitz, R. de Vivie-Riedle, M. Motzkus *et al.*, Science **288**, 824 (2000).
[42] L. Poth and A. W. Castleman, J. Phys. Chem. A **102**, 4075 (1998).
[43] J. K. Kou, V. Zhakhovskii, S. Sakabe *et al.*, J. Chem. Phys. **112**, 5012 (2000).
[44] R. C. Constantinescu, S. Hunsche, H. B. van Linden van den Heuvell, H. G. Muller, C. LeBlanc, and F. Salin, Phys. Rev. A **58**, 4637 (1998).
[45] P. Hering, M. Brewczyk, and C. Cornaggia, Phys. Rev. Lett. **85**, 2288 (2000).
[46] A. N. Markevitch, S. M. Smith, D. A. Romanov, H. B. Schlegel, M. Y. Ivanov, and R. J. Levis, Phys. Rev. A **68**, 011402(R) (2003).
[47] A. N. Markevitch, D. A. Romanov, S. M. Smith, H. B. Schlegel, M. Y. Ivanov, and R. J. Levis, Phys. Rev. A **69**, 013401 (2004).
[48] A. N. Markevitch, N. P. Moore, and R. J. Levis, Chem. Phys. **267**, 131 (2001).

[49] M. A. Walker, P. Hansch, and L. D. Van Woerkom, Phys. Rev. A **57**, R701 (1998).
[50] M. J. DeWitt and R. J. Levis, J. Chem. Phys. **110**, 11368 (1999).
[51] M. J. Frisch, G. W. Trucks, H. B. Schlegel *et al.*, *Gaussian 03, Revision C.02* (Gaussian, Inc., Wallingford, CT, 2004).
[52] J. B. Sutherland, A. L. Selby, J. P. Freeman *et al.*, Mycol. Res. **96**, 509 (1992).
[53] J. D. Moody, J. P. Freeman, D. R. Doerge *et al.*, Appl. Environ. Microbiol. **67**, 1476 (2001).
[54] N. B. Delone and V. P. Krainov, *Atoms in Strong Laser Fields* (Springer-Verlag, Berlin, 1985).
[55] M. Silverstein and F. X. Webster, *Spectrometric Identification of Organic Compounds* (Wiley, New York, 1998).